Experimental violation of a Bell's inequality with efficient detection

M. A. Rowe*, D. Kielpinski*, V. Meyer*, C. A. Sackett*, W. M. Itano*, C. Monroe† & D. J. Wineland*

** Time and Frequency Division, National Institute of Standards and Technology, Boulder, Colorado 80305, USA*
† Department of Physics, University of Michigan, Ann Arbor, Michigan 48109, USA

Local realism is the idea that objects have definite properties whether or not they are measured, and that measurements of these properties are not affected by events taking place sufficiently far away[1]. Einstein, Podolsky and Rosen[2] used these reasonable assumptions to conclude that quantum mechanics is incomplete. Starting in 1965, Bell and others constructed mathematical inequalities whereby experimental tests could distinguish between quantum mechanics and local realistic theories[1,3–5]. Many experiments[1,6–15] have since been done that are consistent with quantum mechanics and inconsistent with local realism. But these conclusions remain the subject of considerable interest and debate, and experiments are still being refined to overcome 'loopholes' that might allow a local realistic interpretation. Here we have measured correlations in the classical properties of massive entangled particles ($^9Be^+$ ions): these correlations violate a form of Bell's inequality. Our measured value of the appropriate Bell's 'signal' is 2.25 ± 0.03, whereas a value of 2 is the maximum allowed by local realistic theories of nature. In contrast to previous measurements with massive particles, this violation of Bell's inequality was obtained by use of a complete set of measurements. Moreover, the high detection efficiency of our apparatus eliminates the so-called 'detection' loophole.

Early experiments to test Bell's inequalities were subject to two primary, although seemingly implausible, loopholes. The first might be termed the locality or 'lightcone' loophole, in which the correlations of apparently separate events could result from unknown subluminal signals propagating between different regions of the apparatus. Aspect[16] has given a brief history of this issue, starting with the experiments of ref. 8 and highlighting the strict relativistic separation between measurements reported by the Innsbruck group[15]. Similar results have also been reported for the Geneva experiment[14,17]. The second loophole is usually referred to as the detection loophole. All experiments up to now have had detection efficiencies low enough to allow the possibility that the subensemble of detected events agrees with quantum mechanics even though the entire ensemble satisfies Bell's inequalities. Therefore it must be assumed that the detected events represent the entire ensemble; a fair-sampling hypothesis. Several proposals for closing this loophole have been made[18–24]; we believe the experiment that we report here is the first to do so. Another feature of our experiment is that it uses massive particles. A previous test of Bell's inequality was carried out on protons[25], but the interpretation of the detected events relied on quantum mechanics, as symmetries valid given quantum mechanics were used to extrapolate the data to a complete set of Bell's angles. Here we do not make such assumptions.

A Bell measurement of the type suggested by Clauser, Horne, Shimony and Holt[5] (CHSH) consists of three basic ingredients (Fig. 1a). First is the preparation of a pair of particles in a repeatable starting configuration (the output of the 'magic' box in Fig. 1a). Second, a variable classical manipulation is applied independently to each particle; these manipulations are labelled ϕ_1 and ϕ_2. Finally, in the detection phase, a classical property with two possible outcomes is measured for each of the particles. The correlation of these outcomes

$$q(\phi_1,\phi_2)=\frac{N_{\text{same}}(\phi_1,\phi_2)-N_{\text{different}}(\phi_1,\phi_2)}{N_{\text{same}}+N_{\text{different}}} \quad (1)$$

is measured by repeating the experiment many times. Here N_{same} and $N_{\text{different}}$ are the number of measurements where the two results were the same and different, respectively. The CHSH form of Bell's inequalities states that the correlations resulting from local realistic theories must obey:

$$B(\alpha_1,\delta_1,\beta_2,\gamma_2)=|q(\delta_1,\gamma_2)-q(\alpha_1,\gamma_2)| + |q(\delta_1,\beta_2)+q(\alpha_1,\beta_2)|\leqslant 2 \quad (2)$$

where α_1 and δ_1 (β_2 and γ_2) are specific values of ϕ_1 (ϕ_2). For example, in a photon experiment[15], parametric down-conversion prepares a pair of photons in a singlet Einstein–Podolsky–Rosen (EPR) pair. After this, a variable rotation of the photon polarization is applied to each photon. Finally, the photons' polarization states, vertical or horizontal, are determined.

Our experiment prepares a pair of two-level atomic ions in a repeatable configuration (entangled state). Next, a laser field is applied to the particles; the classical manipulation variables are the

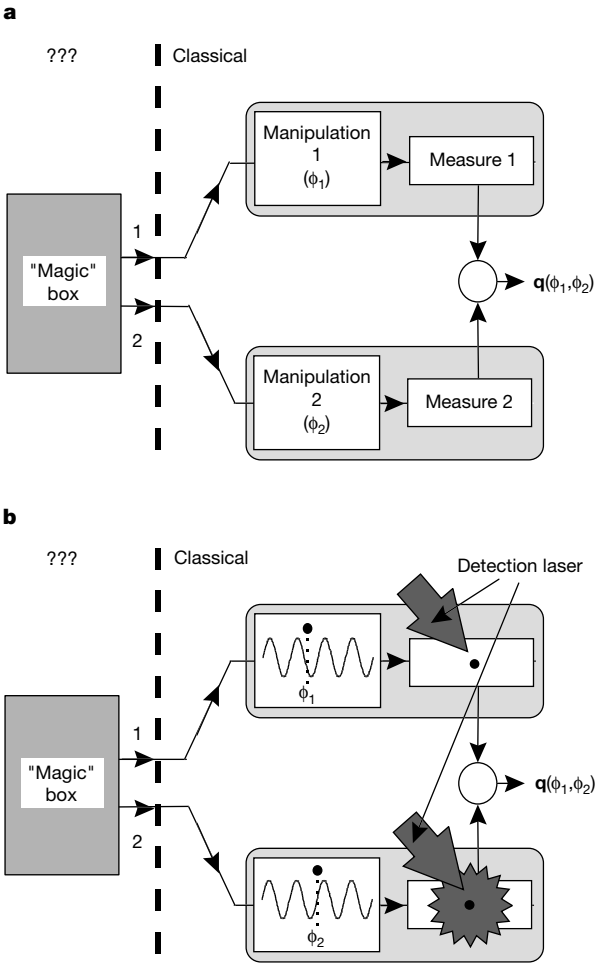

Figure 1 Illustration of how Bell's inequality experiments work. The idea is that a 'magic box' emits a pair of particles. We attempt to determine the joint properties of these particles by applying various classical manipulations to them and observing the correlations of the measurement outputs. **a**, A general CHSH type of Bell's inequality experiment. **b**, Our experiment. The manipulation is a laser wave applied with phases ϕ_1 and ϕ_2 to ion 1 and ion 2 respectively. The measurement is the detection of photons emanating from the ions upon application of a detection laser. Two possible measurement outcomes are possible, detection of few photons (as depicted for ion 1 in the figure) or the detection of many photons (as depicted for ion 2 in the figure).

phases of this field at each ion's position. Finally, upon application of a detection laser beam, the classical property measured is the number of scattered photons emanating from the particles (which effectively measures their atomic states). Figure 1b shows how our experiment maps onto the general case. Entangled atoms produced in the context of cavity-quantum-electrodynamics[26] could similarly be used to measure Bell's inequalities.

The experimental apparatus is as described in ref. 27. Two $^9Be^+$ ions are confined along the axis of a linear Paul trap with an axial centre-of-mass frequency of 5 MHz. We select two resolved levels of the $2S_{1/2}$ ground state, $|\downarrow\rangle \equiv |F = 2, m_F = -2\rangle$ and $|\uparrow\rangle \equiv |F = 1, m_F = -1\rangle$, where F and m_F are the quantum numbers of the total angular momentum. These states are coupled by a coherent stimulated Raman transition. The two laser beams used to drive the transition have a wavelength of 313 nm and a difference frequency near the hyperfine splitting of the states, $\omega_0 \cong 2\pi \times 1.25$ GHz. The beams are aligned perpendicular to each other, with their difference wavevector $\Delta\mathbf{k}$ along the trap axis. As described in ref. 27, it is possible in this configuration to produce the entangled state

$$|\psi_2\rangle = \frac{1}{\sqrt{2}}(|\uparrow\uparrow\rangle - |\downarrow\downarrow\rangle) \quad (3)$$

The fidelity $F = \langle\psi_2|\rho|\psi_2\rangle$, where ρ is the density matrix for the state we make, was about 88% for the data runs. In the discussion below we assume $|\psi_2\rangle$ as the starting condition for the experiment.

After making the state $|\psi_2\rangle$, we again apply Raman beams for a pulse of short duration (~400 ns) so that the state of each ion j is transformed in the interaction picture as

$$|\uparrow_j\rangle \rightarrow \frac{1}{\sqrt{2}}(|\uparrow_j\rangle - ie^{-i\phi_j}|\downarrow_j\rangle); |\downarrow_j\rangle \rightarrow \frac{1}{\sqrt{2}}(|\downarrow_j\rangle - ie^{i\phi_j}|\uparrow_j\rangle) \quad (4)$$

The phase, ϕ_j, is the phase of the field driving the Raman transitions (more specifically, the phase difference between the two Raman beams) at the position of ion j and corresponds to the inputs ϕ_1 and ϕ_2 in Fig. 1. We set this phase in two ways in the experiment. First, as an ion is moved along the trap axis this phase changes by $\Delta\mathbf{k}\cdot\Delta\mathbf{x}_j$. For example, a translation of $\lambda/\sqrt{2}$ along the trap axis corresponds to a phase shift of 2π. In addition, the laser phase on both ions is changed by a common amount by varying the phase, ϕ_s, of the radio-frequency synthesizer that determines the Raman difference frequency. The phase on ion j is therefore

$$\phi_j = \phi_s + \Delta\mathbf{k}\cdot\mathbf{x}_j \quad (5)$$

In the experiment, the axial trap strength is changed so that the ions move about the centre of the trap symmetrically, giving $\Delta x_1 = -\Delta x_2$. Therefore the trap strength controls the differential phase, $\Delta\phi \equiv \phi_1 - \phi_2 = \Delta\mathbf{k}\cdot(\mathbf{x}_1 - \mathbf{x}_2)$, and the synthesizer controls the total phase, $\phi_{tot} \equiv \phi_1 + \phi_2 = 2\phi_s$. The calibration of these relations is discussed in the Methods.

The state of an ion, $|\downarrow\rangle$ or $|\uparrow\rangle$, is determined by probing the ion with circularly polarized light from a 'detection' laser beam[27]. During this detection pulse, ions in the $|\downarrow\rangle$ or bright state scatter many photons, and on average about 64 of these are detected with a photomultiplier tube, while ions in the $|\uparrow\rangle$ or dark state scatter very few photons. For two ions, three cases can occur: zero ions bright, one ion bright, or two ions bright. In the one-ion-bright case it is not necessary to know which ion is bright because the Bell's measurement requires only knowledge of whether or not the ions' states are different. Figure 2 shows histograms, each with 20,000 detection measurements. The three cases are distinguished from each other with simple discriminator levels in the number of photons collected with the phototube.

An alternative description of our experiment can be made in the language of spin-one-half magnetic moments in a magnetic field (directed in the $\hat{z}$ direction). The dynamics of the spin system are the same as for our two-level system[28]. Combining the manipulation (equation (4)) and measurement steps, we effectively measure the spin projection of each ion j in the $\hat{r}_j$ direction, where the vector $\hat{r}_j$ is in the $\hat{x} - \hat{y}$ plane at an angle ϕ_j to the $\hat{y}$ axis. Although we have used quantum-mechanical language to describe the manipulation and measurement steps, we emphasize that both are procedures completely analogous to the classical rotations of wave-plates and measurements of polarization in an optical apparatus.

Here we calculate the quantum-mechanical prediction for the correlation function. Our manipulation step transforms the starting

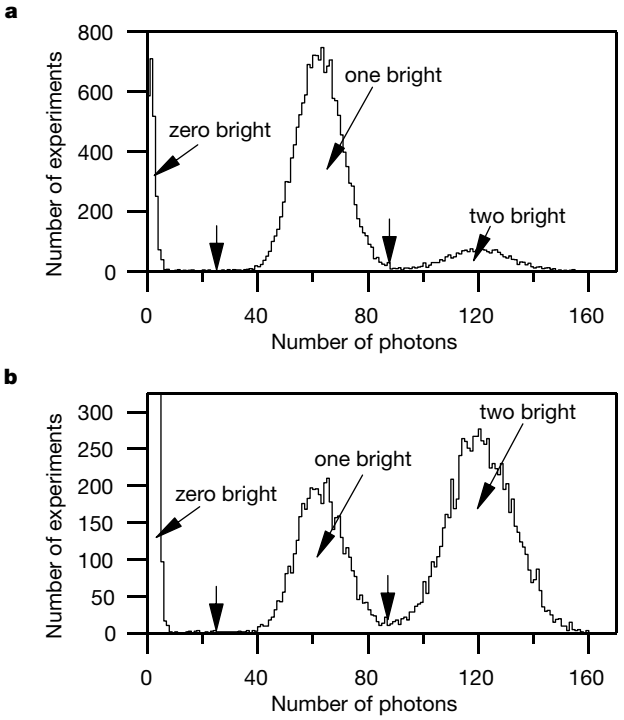

Figure 2 Typical data histograms comprising the detection measurements of 20,000 experiments taking a total time of about 20 s. In each experiment the population in the $|\uparrow\rangle$ state is first coherently transferred to the $|F = 1, M_F = +1\rangle$ to make it even less likely to fluoresce upon application of the detection laser. The detection laser is turned on and the number of fluorescence photons detected by the phototube in 1 ms is recorded. The cut between the one bright and two bright cases is made so that the fractions of two equal distributions which extend past the cut points are equal. The vertical arrows indicate the location of the cut between the 0 (1) bright and 1 (2) bright peaks at 25 (86) counts. **a**, Data histogram with a negative correlation using $\phi_1 = 3\pi/8$ and $\phi_2 = 3\pi/8$. For these data $N_0 \cong 2{,}200$, $N_1 \cong 15{,}500$ and $N_2 \cong 2{,}300$. **b**, Data histogram with a positive correlation using $\phi_1 = 3\pi/8$ and $\phi_2 = -\pi/8$. For these data $N_0 \cong 7{,}700$, $N_1 \cong 4{,}400$ and $N_2 \cong 7{,}900$. The zero bright peak extends vertically to 2,551.

Table 1 The four sets of phase angles used for the Bell's experiment

Experiment input	ϕ_1	ϕ_2	$\Delta\phi$	ϕ_{tot}
$\alpha_1\beta_2$	$-\pi/8$	$-\pi/8$	0	$-\pi/4$
$\alpha_1\gamma_2$	$-\pi/8$	$3\pi/8$	$-\pi/2$	$+\pi/4$
$\delta_1\beta_2$	$3\pi/8$	$-\pi/8$	$+\pi/2$	$+\pi/4$
$\delta_1\gamma_2$	$3\pi/8$	$3\pi/8$	0	$+3\pi/4$

Table 2 Correlation values and resulting Bell's signals for five experimental runs

Run number	$q(\alpha_1, \beta_2)$	$q(\alpha_1, \gamma_2)$	$q(\delta_1, \beta_2)$	$q(\delta_1, \gamma_2)$	$B(\alpha_1, \delta_1, \beta_2, \gamma_2)$
1	0.541	0.539	0.569	–0.573	2.222
2	0.575	0.570	0.530	–0.600	2.275
3	0.551	0.634	0.590	–0.487	2.262
4	0.575	0.561	0.559	–0.551	2.246
5	0.541	0.596	0.537	–0.571	2.245

The experimental angle values were $\alpha_1 = -(\pi/8)$, $\delta_1 = 3\pi/8$, $\beta_2 = -(\pi/8)$, and $\gamma_2 = 3\pi/8$. The statistical errors are 0.006 and 0.012 for the q and B values respectively. The systematic errors (see text) are 0.03 and 0.06 for the q and B values respectively.

state, $|\psi_2\rangle$, to

$$|\psi_2'\rangle = \frac{1}{2\sqrt{2}}\{(1+e^{i(\phi_1+\phi_2)})(|\uparrow\uparrow\rangle - e^{-i(\phi_1+\phi_2)}|\downarrow\downarrow\rangle) - i(1-e^{i(\phi_1+\phi_2)})(e^{-i\phi_2}|\uparrow\downarrow\rangle + e^{-i\phi_1}|\downarrow\uparrow\rangle)\} \quad (6)$$

Using the measurement operators $\hat{N}_{\text{same}} = N_{\text{tot}}[|\uparrow\uparrow\rangle\langle\uparrow\uparrow| + |\downarrow\downarrow\rangle\langle\downarrow\downarrow|]$ and $\hat{N}_{\text{different}} = N_{\text{tot}}[|\uparrow\downarrow\rangle\langle\uparrow\downarrow| + |\downarrow\uparrow\rangle\langle\downarrow\uparrow|]$, the correlation function is calculated to be

$$q(\phi_1,\phi_2) = \frac{1}{8}[2|1+e^{i(\phi_1+\phi_2)}|^2 - 2|1-e^{i(\phi_1+\phi_2)}|^2] = \cos(\phi_1+\phi_2) \quad (7)$$

The CHSH inequality (equation (2)) is maximally violated by quantum mechanics at certain sets of phase angles. One such set is $\alpha_1 = -(\pi/8)$, $\delta_1 = 3\pi/8$, $\beta_2 = -(\pi/8)$ and $\gamma_2 = 3\pi/8$. With these phase angles quantum mechanics predicts

$$B\left(-\frac{\pi}{8},\frac{3\pi}{8},-\frac{\pi}{8},\frac{3\pi}{8}\right) = 2\sqrt{2} \quad (8)$$

This violates the local realism condition, which requires that $B \leqslant 2$.

The correlation function is measured experimentally at four sets of phase angles, listed in Table 1. The experiment is repeated $N_{\text{tot}} = 20{,}000$ times at each of the four sets of phases. For each set of phases the correlation function is calculated using

$$q = \frac{(N_0+N_2)-N_1}{N_{\text{tot}}} \quad (9)$$

Here N_0, N_1 and N_2 are the number of events with zero, one and two ions bright, respectively. The correlation values from the four sets of phase angles are combined into the Bell's signal, $B(\alpha_1,\delta_1,\beta_2,\gamma_2)$, using equation (2). The correlation values and resulting Bell's signals from five data runs are given in Table 2.

So far we have described the experiment in terms of perfect implementation of the phase angles. In the actual experiment, however, α_1, δ_1, β_2 and γ_2 are not quite the same angles both times they occur in the Bell's inequality. In our experiment the dominant reason for this error results from the phase instability of the synthesizer, which can cause the angles to drift appreciably during four minutes, the time required to take a complete set of measurements. This random drift causes a root-mean-squared error for the correlation function of ± 0.03 on this timescale, which propagates to an error of ± 0.06 for the Bell's signal. The error for the Bell's signal from the five combined data sets is then ± 0.03, consistent with the run-to-run variation observed. Averaging the five Bell's signals from Table 2, we arrive at our experimental result, which is

$$B\left(-\frac{\pi}{8},\frac{3\pi}{8},-\frac{\pi}{8},\frac{3\pi}{8}\right) = 2.25 \pm 0.03 \quad (10)$$

If we take into account the imperfections of our experiment (imperfect state fidelity, manipulations, and detection), this value agrees with the prediction of quantum mechanics.

The result above was obtained using the outcomes of every experiment, so that no fair-sampling hypothesis is required. In this case, the issue of detection efficiency is replaced by detection accuracy. The dominant cause of inaccuracy in our state detection comes from the bright state becoming dark because of optical pumping effects. For example, imperfect circular polarization of the detection light allows an ion in the $|\downarrow\rangle$ state to be pumped to $|\uparrow\rangle$, resulting in fewer collected photons from a bright ion. Because of such errors, a bright ion is misidentified 2% of the time as being dark. This imperfect detection accuracy decreases the magnitude of the measured correlations. We estimate that our Bell's signal would be 2.37 with perfect detection accuracy.

We have thus presented experimental results of a Bell's inequality measurement where a measurement outcome was recorded for every experiment. Our detection efficiency was high enough for a Bell's inequality to be violated without requiring the assumption of fair sampling, thereby closing the detection loophole in this experiment. The ions were separated by a distance large enough that no known interaction could affect the results; however, the lightcone loophole remains open here. Further details of this experiment will be published elsewhere. □

Methods

Phase calibration

The experiment was run with specific phase differences of the Raman laser beam fields at each ion. In order to implement a complete set of laser phases, a calibration of the phase on each ion as a function of axial trap strength was made. We emphasize that the calibration method is classical in nature. Although quantum mechanics guided the choice of calibration method, no quantum mechanics was used to interpret the signal. General arguments are used to describe the signal resulting from a sequence of laser pulses and its dependence on the classical physical parameters of the system, the laser phase at the ion, and the ion's position.

In the calibration procedure, a Ramsey experiment was performed on two ions. The first $\pi/2$ Rabi rotation was performed identically each time. The laser phases at the ions' positions for the second $\pi/2$ Rabi rotation were varied, ϕ_1 for ion 1 and ϕ_2 for ion 2. The detection signal is the total number of photons counted during detection. With an auxiliary one-ion experiment we first established empirically that the individual signal depends only on the laser phase at an individual ion and is $C + A\cos\phi_i$. Here C and A are the offset and amplitude of the one-ion signal. We measure the detector to be linear, so that the detection signal is the sum of the two ions' individual signals. The two-ion signal is therefore

$$C + A\cos\phi_1 + C + A\cos\phi_2 = 2C + 2A\cos\left[\frac{1}{2}(\phi_1+\phi_2)\right]\cos\left[\frac{1}{2}(\phi_1-\phi_2)\right] \quad (11)$$

By measuring the fringe amplitude and phase as $\phi_s = (\phi_1+\phi_2)/2$ is swept, we calibrate $\phi_1 - \phi_2$ as a function of trap strength and ensure that $\phi_1 + \phi_2$ is independent of trap strength.

We use the phase convention that at the ion separation used for the entanglement preparation pulse the maximum of the correlation function is at $\phi_1 = \phi_2 = 0$ (or $\Delta\phi = \phi_{\text{tot}} = 0$). Our measurement procedure begins by experimentally finding this condition of $\phi_1 = \phi_2 = 0$ by keeping $\Delta\phi = 0$ and scanning the synthesizer phase to find the maximum correlation. The experiment is then adjusted to the phase angles specified above by switching the axial trap strength to set $\Delta\phi$ and incrementing the synthesizer phase to set ϕ_{tot}.

Locality issues

The ions are separated by a distance of approximately 3 μm, which is greater than 100 times the size of the wavepacket of each ion. Although the Coulomb interaction strongly couples the ions' motion it does not affect the ions' internal states. At this distance, all known relevant interactions are expected to be small. For example, dipole–dipole interactions between the ions slightly modify the light-scattering intensity, but this effect is negligible for the ion–ion separations used[29]. Also, the detection solid angle is large enough that Young's interference fringes, if present, are averaged out[30]. Even though all known interactions would cause negligible correlations in the measurement outcomes, the ion separation is not large enough to eliminate the lightcone loophole.

We note that the experiment would be conceptually simpler if, after creating the entangled state, we separated the ions so that the input manipulations and measurements were done individually. However, unless we separated the ions by a distance large enough to overcome the lightcone loophole, this is only a matter of convenience of description and does not change the conclusions that can be drawn from the results.

Received 25 October; accepted 30 November 2000.

1. Clauser, J. F. & Shimony, A. Bell's theorem: experimental tests and implications. *Rep. Prog. Phys.* **41,** 1883–1927 (1978).
2. Einstein, A., Podolsky, B. & Rosen, N. Can quantum-mechanical description of reality be considered complete? *Phys. Rev.* **47,** 777–780 (1935).
3. Bell, J. S. On the Einstein-Podolsky-Rosen paradox. *Physics* **1,** 195–200 (1965).
4. Bell, J. S. in *Foundations of Quantum Mechanics* (ed. d'Espagnat, B.) 171–181 (Academic, New York, 1971).
5. Clauser, J. F., Horne, M. A., Shimony, A. & Holt, R. A. Proposed experiment to test local hidden-variable theories. *Phys. Rev. Lett.* **23,** 880–884 (1969).
6. Freedman, S. J. & Clauser, J. F. Experimental test of local hidden-variable theories. *Phys. Rev. Lett.* **28,** 938–941 (1972).
7. Fry, E. S. & Thompson, R. C. Experimental test of local hidden-variable theories. *Phys. Rev. Lett.* **37,** 465–468 (1976).
8. Aspect, A., Grangier, P. & Roger, G. Experimental realization of Einstein-Podolsky-Rosen-Bohm *Gedankenexperiment*: a new violation of Bell's inequalities. *Phys. Rev. Lett.* **49,** 91–94 (1982).
9. Aspect, A., Dalibard, J. & Roger, G. Experimental test of Bell's inequalities using time-varying analyzers. *Phys. Rev. Lett.* **49,** 1804–1807 (1982).
10. Ou, Z. Y. & Mandel, L. Violation of Bell's inequality and classical probability in a two-photon correlation experiment. *Phys. Rev. Lett.* **61,** 50–53 (1988).
11. Shih, Y. H. & Alley, C. O. New type of Einstein-Podolsky-Rosen-Bohm experiment using pairs of light

quanta produced by optical parametric down conversion. *Phys. Rev. Lett.* **61,** 2921–2924 (1988).
12. Tapster, P. R., Rarity, J. G. & Owens, P. C. M. Violation of Bell's inequality over 4 km of optical fiber. *Phys. Rev. Lett.* **73,** 1923–1926 (1994).
13. Kwiat, P. G., Mattle, K., Weinfurter, H. & Zeilinger, A. New high-intensity source of polarization-entangled photon pairs. *Phys. Rev. Lett.* **75,** 4337–4341 (1995).
14. Tittel, W., Brendel, J., Zbinden, H. & Gisin, N. Violation of Bell inequalities by photons more than 10 km apart. *Phys. Rev. Lett.* **81,** 3563–3566 (1998).
15. Weihs, G. *et al.* Violation of Bell's inequality under strict Einstein locality conditions. *Phys. Rev. Lett.* **81,** 5039–5043 (1998).
16. Aspect, A. Bell's inequality test: more ideal than ever. *Nature* **398,** 189–190 (1999).
17. Gisin, N. & Zbinden, H. Bell inequality and the locality loophole: active versus passive switches. *Phys. Lett. A* **264,** 103–107 (1999).
18. Lo, T. K. & Shimony, A. Proposed molecular test of local hidden-variable theories. *Phys. Rev. A* **23,** 3003–3012 (1981).
19. Kwiat, P. G., Eberhard, P. H., Steinberg, A. M. & Chiao, R. Y. Proposal for a loophole-free Bell inequality experiment. *Phys. Rev. A* **49,** 3209–3220 (1994).
20. Huelga, S. F., Ferrero, M. & Santos, E. Loophole-free test of the Bell inequality. *Phys. Rev. A* **51,** 5008–5011 (1995).
21. Fry, E. S., Walther, T. & Li, S. Proposal for a loophole free test of the Bell inequalities. *Phys. Rev. A* **52,** 4381–4395 (1995).
22. Freyberger, M., Aravind, P. K., Horne, M. A. & Shimony, A. Proposed test of Bell's inequality without a detection loophole by using entangled Rydberg atoms. *Phys. Rev. A* **53,** 1232–1244 (1996).
23. Brif, C. & Mann, A. Testing Bell's inequality with two-level atoms via population spectroscopy. *Europhys. Lett.* **49,** 1–7 (2000).
24. Beige, A., Munro, W. J. & Knight, P. L. A Bell's inequality test with entangled atoms. *Phys. Rev. A* **62,** 052102-1–052102-9 (2000).
25. Lamehi-Rachti, M. & Mittig, W. Quantum mechanics and hidden variables: a test of Bell's inequality by the measurement of the spin correlation in low-energy proton–proton scattering. *Phys. Rev. D* **14,** 2543–2555 (1976).
26. Hagley, E. *et al.* Generation of Einstein-Podolsky-Rosen pairs of atoms. *Phys. Rev. Lett.* **79,** 1–5 (1997).
27. Sackett, C. A. *et al.* Experimental entanglement of four particles. *Nature* **404,** 256–259 (2000).
28. Feynman, R. P., Vernon, F. L. & Hellwarth, R. W. Geometrical representation of the Schrödinger equation for solving maser problems. *J. Appl. Phys.* **28,** 49–52 (1957).
29. Richter, T. Cooperative resonance fluorescence from two atoms experiencing different driving fields. *Optica Acta* **30,** 1769–1780 (1983).
30. Eichmann, U. *et al.* Young's interference experiment with light scattered from two atoms. *Phys. Rev. Lett.* **70,** 2359–2362 (1993).

Acknowledgements

We thank A. Ben-Kish, J. Bollinger, J. Britton, N. Gisin, P. Knight, P. Kwiat and I. Percival for useful discussions and comments on the manuscript. This work was supported by the US National Security Agency (NSA) and the Advanced Research and Development Activity (ARDA), the US Office of Naval Research, and the US Army Research Office. This paper is a contribution of the National Institute of Standards and Technology and is not subject to US copyright.

Correspondence and requests for materials should be addressed to D.J.W. (e-mail: david.wineland@boulder.nist.gov).

Autonomic healing of polymer composites

S. R. White*, N. R. Sottos†, P. H. Geubelle*, J. S. Moore‡, M. R. Kessler†, S. R. Sriram‡, E. N. Brown† & S. Viswanathan*

* *Department of Aeronautical and Astronautical Engineering,* † *Department of Theoretical and Applied Mechanics,* ‡ *Department of Chemistry, University of Illinois at Urbana-Champaign, Urbana, Illinois 61801, USA*

Structural polymers are susceptible to damage in the form of cracks, which form deep within the structure where detection is difficult and repair is almost impossible. Cracking leads to mechanical degradation[1–3] of fibre-reinforced polymer composites; in microelectronic polymeric components it can also lead to electrical failure[4]. Microcracking induced by thermal and mechanical fatigue is also a long-standing problem in polymer adhesives[5]. Regardless of the application, once cracks have formed within polymeric materials, the integrity of the structure is significantly compromised. Experiments exploring the concept of self-repair have been previously reported[6–8], but the only successful crack-healing methods that have been reported so far require some form of manual intervention[10–18]. Here we report a structural polymeric material with the ability to autonomically heal cracks. The material incorporates a microencapsulated healing agent that is released upon crack intrusion. Polymerization of the healing agent is then triggered by contact with an embedded catalyst, bonding the crack faces. Our fracture experiments yield as much as 75% recovery in toughness, and we expect that our approach will be applicable to other brittle materials systems (including ceramics and glasses).

Figure 1 illustrates our autonomic healing concept. Healing is accomplished by incorporating a microencapsulated healing agent and a catalytic chemical trigger within an epoxy matrix. An approaching crack ruptures embedded microcapsules, releasing healing agent into the crack plane through capillary action. Polymerization of the healing agent is triggered by contact with the embedded catalyst, bonding the crack faces. The damage-induced triggering mechanism provides site-specific autonomic control of repair. An additional unique feature of our healing concept is the use of living (that is, having unterminated chain-ends) polymerization catalysts, thus enabling multiple healing events. Engineering this self-healing composite involves the challenge of combining polymer science, experimental and analytical mechanics, and composites processing principles.

We began by analysing the effects of microcapsule geometry and properties on the mechanical triggering process. For example, capsule walls that are too thick will not rupture when the crack approaches, whereas capsules with very thin walls will break during processing. Other relevant design parameters are the toughness and the relative stiffness of the microcapsules, and the strength of the interface between the microcapsule and the matrix. Micromechanical modelling with the aid of the Eshelby–Mura equivalent inclusion method[19] has been used to study various aspects of the complex three-dimensional interaction between a crack and a microcapsule. An illustrative result from these studies is presented in Fig. 2a, which shows the effect of the relative stiffness of the microcapsule on the propagation path of an approaching crack. The crack, the sphere and the surrounding matrix are subjected to a far-field tensile loading, σ_∞, perpendicular to the crack plane.

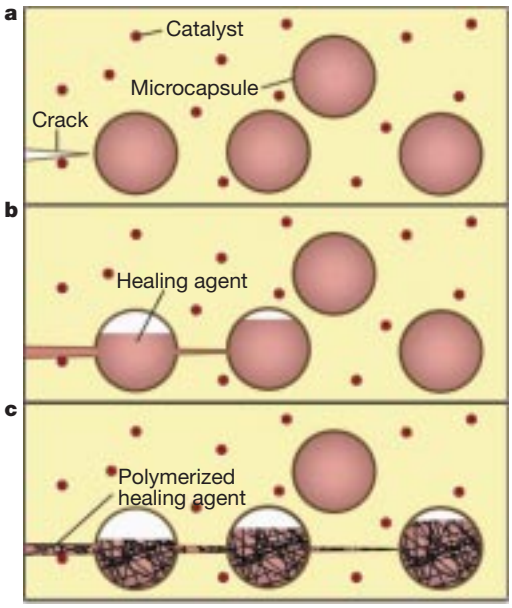

Figure 1 The autonomic healing concept. A microencapsulated healing agent is embedded in a structural composite matrix containing a catalyst capable of polymerizing the healing agent. **a**, Cracks form in the matrix wherever damage occurs; **b**, the crack ruptures the microcapsules, releasing the healing agent into the crack plane through capillary action; **c**, the healing agent contacts the catalyst, triggering polymerization that bonds the crack faces closed.